SCIENTIFIC REPORTS

OPEN

Influence of interstitial Fe to the phase diagram of $Fe_{1+y}Te_{1-x}Se_x$ single crystals

Yue Sun, Tatsuhiro Yamada, Sunseng Pyon & Tsuyoshi Tamegai

Superconductivity (SC) with the suppression of long-range antiferromagnetic (AFM) order is observed in the parent compounds of both iron-based and cuprate superconductors. The AFM wave vectors are bicollinear (π, 0) in the parent compound FeTe different from the collinear AFM order (π, π) in most iron pnictides. Study of the phase diagram of $Fe_{1+y}Te_{1-x}Se_x$ is the most direct way to investigate the competition between bicollinear AFM and SC. However, presence of interstitial Fe affects both magnetism and SC of $Fe_{1+y}Te_{1-x}Se_x$, which hinders the establishment of the real phase diagram. Here, we report the comparison of doping-temperature (x-T) phase diagrams for $Fe_{1+y}Te_{1-x}Se_x$ ($0 \leq x \leq 0.43$) single crystals before and after removing interstitial Fe. Without interstitial Fe, the AFM state survives only for $x < 0.05$, and bulk SC emerges from $x = 0.05$, and does not coexist with the AFM state. The previously reported spin glass state, and the coexistence of AFM and SC may be originated from the effect of the interstitial Fe. The phase diagram of $Fe_{1+y}Te_{1-x}Se_x$ is found to be similar to the case of the "1111" system such as $LaFeAsO_{1-x}F_x$, and is different from that of the "122" system.

The discovery of superconductivity (SC) in iron-based superconductors (IBSs)[1] provides another route to realize SC at high temperatures other than the cuprates. Some similarities between IBSs and cuprates give us important clues to the understanding of the mechanism of high temperature SC. Among those similarities like layered structure and very high critical field[2], the most important aspect is that both systems maintain a long-range antiferromagnetic (AFM) order in the parent compounds, and the SC emerges after the suppression of the AFM order[3]. Thus, the study of phase diagram becomes the most direct way to investigate the relation between AFM and SC. Until now, integrated phase diagrams for some members of IBSs have already been well established, especially in the "122" system since single crystals with sufficient dimensions and good quality can be obtained easily[4]. Some interesting phenomena are observed like the coexistence of AFM and SC in under-doped region[4], asymmetric superconducting dome in $Ba_{1-x}K_xFe_2As_2$[5], nematic orders[6] and quantum critical point (QCP)[7]. All these discoveries in the past several years have promoted our understanding of the mechanism of SC in IBSs. Spin fluctuations related to the nesting of disconnected electron and hole Fermi surfaces[8], are proposed to be responsible for the high value of T_c in IBSs based on the $s_\pm$ scenario[9]. In addition, the contribution of large orbital fluctuation has also been stressed from the s_{++} scenario[10].

On the other hand, iron chalcogenides recently attracted much more attention in IBSs because of its unexpected high T_c. Although the initial T_c in FeSe was only 8 K[11], it increased up to 14 K[12] with appropriate Te substitution and up to 37 K[13,14] under high pressure. Furthermore, by intercalating spacer layers between adjacent FeSe layers, T_c has reached ~32 K[15] in $A_xFe_{2-y}Se_2$ (A = K, Cs, Rb and Tl) and 43 K[16] in $Li_x(NH_2)_y(NH_3)_{1-y}Fe_2Se_2$ ($x \sim 0.6$; $y \sim 0.2$). By applying pressure to $A_xFe_{2-y}Se_2$, T_c can even reach ~48 K[17]. Furthermore, the monolayer of FeSe grown on $SrTiO_3$ even shows a sign of SC over 100 K[18]. Among iron chalcogenides, $Fe_{1+y}Te_{1-x}Se_x$ is unique in its structural simplicity, consisting of only iron-chalcogenide layers, which is ideal for probing the mechanism of SC. Although $Fe_{1+y}Te_{1-x}Se_x$ shows some similarities to iron pnictides like the Fermi surface topology which is characterized by hole bands around Γ point and electron bands around M point[8], it manifests some unique properties different from iron pnictides. The most crucial one is the antiferromagnetic wave vectors, which is bicollinear (π, 0) in the parent compound FeTe[19] different from the collinear antiferromagnetic order (π, π) in most of iron pnictides[20]. Since the AFM order is believed to be related to the high temperature SC, a systematic study of the competition between bicollinear AFM and SC orders with doping is crucial to the understanding of

Department of Applied Physics, The University of Tokyo, 7-3-1 Hongo, Bunkyo-ku, Tokyo 113-8656, Japan. Correspondence and requests for materials should be addressed to Y.S. (email: sunyue.seu@gmail.com)
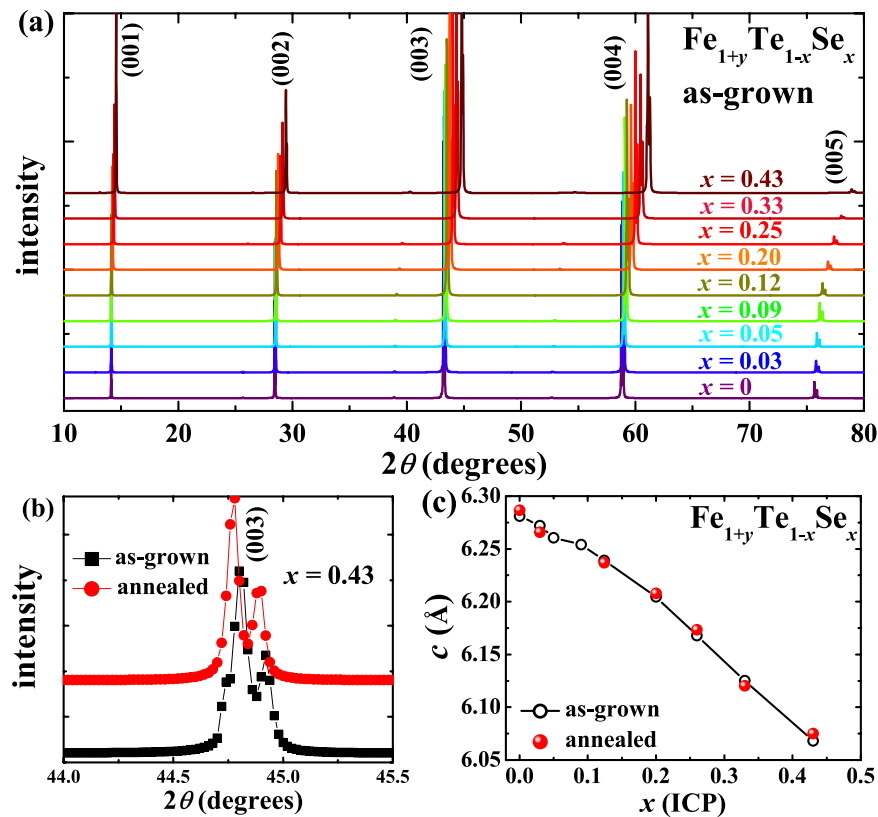
Figure 1. (**a**) Single crystal X-ray diffraction patterns of the as-grown $Fe_{1+y}Te_{1-x}Se_x$ ($0 \le x \le 0.43$) single crystals. (**b**) Comparison of the (003) peaks for the as-grown and O_2-annealed $Fe_{1+y}Te_{0.57}Se_{0.43}$. (**c**) Lattice constant c for $Fe_{1+y}Te_{1-x}Se_x$ before and after annealing.

its paring mechanism. Furthermore, the phase diagram of $Fe_{1+y}Te_{1-x}Se_x$ will give us another opportunity to testify some phenomena observed in iron pnictides like the coexistence of AFM and SC, and the possible QCP.

Until now, although several phase diagrams have been already reported based on $Fe_{1+y}Te_{1-x}Se_x$ single crystals[21–25] and even thin films[26,27], they are all under debate, especially in the low Se doping region. Some basic information is even controversial in those reported results, like the region of bulk SC, the coexistence of AFM and SC, and the spin glass state. These controversies are believed to come from the sample-dependent Fe non-stoichiometries[19,28], which originate from the partial occupation of the second Fe site (interstitial Fe site) in the Te/Se layer. The interstitial Fe with valence near Fe^+ will provide an electron into the 11 system[29]. The interstitial Fe is also strongly magnetic, which provides local moments that interact with the adjacent Fe layers[29]. In the parent compound $Fe_{1+y}Te$, the long-range (π, 0) order can be tuned from commensurate to incommensurate by changing the amount of interstitial Fe[19]. Furthermore, the magnetic moment from interstitial Fe will act as a pair breaker and also localize the charge carriers[30,31]. Thus, the existence of interstitial Fe, which is easily formed in the standard growth technique employing slow cooling and their amount varies among different groups[32], makes the phase diagram of $Fe_{1+y}Te_{1-x}Se_x$ still unclear until now.

Recently, our O_2-annealing technique with fine tuning capability was proved to be very effective in minimizing the detrimental effect of the interstitial Fe and inducing bulk SC with a large value of normalized specific heat jump at T_c[33]. In this report, we adopt the O_2-annealing technique to $Fe_{1+y}Te_{1-x}Se_x$ single crystals with doping level $0 \le x \le 0.43$ to minimize the effect of the interstitial Fe. The doping-temperature (x-T) phase diagrams for $Fe_{1+y}Te_{1-x}Se_x$ ($0 \le x \le 0.43$) single crystals before and after removing interstitial Fe were established and compared based on the systematic studies of the structure, magnetic, and transport properties. Results show that the phase diagram is largely affected by the amount of interstitial Fe for all the doping levels. Without interstitial Fe, the AFM state is found to survive only in a narrow region of $x < 0.05$, and bulk SC emerges from $x = 0.05$, and does not coexist with the AFM state. The previously reported spin glass state, and the coexistence of AFM and SC may be originated from the effect of interstitial Fe. The phase diagram of $FeTe_{1-x}Se_x$ after removing the interstitial Fe is found to be similar to the case of the "1111" system such as $LaFeAsO_{1-x}F_x$[34], and is different from that of the "122" system.

Results

Figure 1(a) shows the single crystal XRD patterns for the as-grown $Fe_{1+y}Te_{1-x}Se_x$ ($0 \le x \le 0.43$) single crystals. Here, the selenium content x is the analyzed value for a similar piece of crystal taken from the same batch by the inductively-coupled plasma (ICP) atomic emission spectroscopy measurements. Only the (00l) peaks are observed, suggesting that the crystallographic c-axis is perfectly perpendicular to the plane of the single crystal.
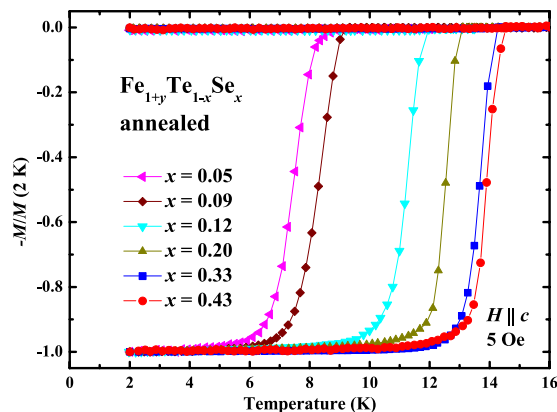
Figure 2. Temperature dependence of zero-field-cooled (ZFC) and field-cooled (FC) magnetization at 5 Oe for the O_2-annealed $Fe_{1+y}Te_{1-x}Se_x$ ($0.05 \leq x \leq 0.43$) single crystals.

With increasing Se doping, the positions of (00l) peaks gradually shift to higher values of 2θ. The lattice constant c is calculated and plotted in Fig. 1(c), which is almost linearly decreasing with increasing Se doping similar to that reported in a previous report[35]. After removing the interstitial Fe by O_2-annealing, the positions for (00l) peaks change little, as shown in Fig. 1(b) for a typical example of (003) peaks for $Fe_{1+y}Te_{0.57}Se_{0.43}$ before and after annealing. The lattice constant c for the annealed crystals is also plotted and compared in Fig. 1(c), which shows that the interstitial Fe affects little to the c-axis lattice constant. Actually, previous analyses proved that the lattice constant a/b is slightly decreased after removing the interstitial Fe, although the lattice constant c changes little[36].

To probe the influence of Se doping to the SC in $Fe_{1+y}Te_{1-x}Se_x$, temperature dependence of zero-field-cooled (ZFC) and field-cooled (FC) magnetization at 5 Oe were measured for the as-grown and annealed crystals. All the as-grown crystals usually show no SC or very weak diamagnetic signal. After removing the interstitial Fe by annealing, SC emerges from $x = 0.05$, and the value of T_c is gradually enhanced with the increase of Se doping up to 14.5 K in $Fe_{1+y}Te_{0.57}Se_{0.43}$ as shown in Fig. 2. Besides, all the annealed crystals show relatively sharp SC transition width $\Delta T_c \leq 1$ K. The SC observed in the annealed crystals has already been proved to be in bulk nature by the clear specific heat jump and a large value of critical current density, J_c, in our previous report[33]. Actually, when the Se doping level is equal or larger than 0.05, all the annealed crystals show large value of $J_c \sim 3 \times 10^5$ A/cm^2 at 2 K under self-field similar to that reported for the crystal with $x = 0.43$[37,38].

Figure 3(a,b) show the normalized magnetic susceptibilities measured under 10 kOe magnetic field parallel to c-axis for the as-grown and annealed $Fe_{1+y}Te_{1-x}Se_x$ ($0 \leq x \leq 0.43$) single crystals, respectively. It is obvious that the as-grown $Fe_{1+y}Te$ shows a sharp transition at ~58 K, which is due to the antiferromagnetic (AFM) transition based on the previous report[23]. With Se doping, the AFM transition temperature T_N is gradually suppressed to lower temperatures, and becomes much broader at $x = 0.09$. After that, the AFM transition disappears and is replaced by a very broad hump-like feature. Such a hump-like feature may be originated from the spin glass state according to the neutron scattering results[21]. The hump-like feature survives up to $x = 0.33$, and is not observed for $x \geq 0.43$.

In crystals after annealing, the value of magnetic susceptibility does not show a systematic evolution and is irregular, which is caused by the magnetism from some Fe impurities. During the annealing process, the interstitial Fe are removed from their original positions (interstitial sites in Te/Se layers), and form some compounds like Fe_2O_3 or $FeTe_2$[33,39,40]. Although those impurities are mainly formed in the surface layers, and removed by polishing before measurements, small parts may still remain inside the crystals and disturb the magnetic susceptibility value because of their strong magnetism. However, we can still obtain some important information from the data regardless of the irregularity in the absolute value. As shown clearly in Fig. 3(b), the value of T_N for the pure FeTe is enhanced to ~72 K after removing the interstitial Fe. The AFM transition is only observed in crystals with $x = 0$ and 0.03. When the Se doping level is increased over 0.05, the AFM is totally suppressed. On the other hand, the hump-like feature observed in the as-grown crystals is not witnessed after annealing. For $x > 0.03$, the annealed crystals only show the SC transition at low temperatures.

Figure 4 shows the temperature dependence of the in-plane resistivity $\rho(T)$ for the as-grown and annealed $Fe_{1+y}Te_{1-x}Se_x$ ($0 \leq x \leq 0.43$) single crystals. For the as-grown crystals, the AFM transition can be observed in the doping region of $0 \leq x \leq 0.05$ as indicated by the solid magenta arrows. The values of T_N are close to those obtained from magnetic susceptibility measurements. For $x \geq 0.05$, the SC transition can be observed and indicated by the dashed blue arrows. However, the SC can be only observed in the resistivity measurements. Neither the diamagnetic signal nor the jump at T_c in specific heat can be observed, which indicates that the SC observed here is filamentary in nature[33]. Furthermore, temperature dependence of resistivity for all the as-grown crystals manifests a nonmetallic behavior ($d\rho/dT < 0$) with decreasing temperature below 150 K. Such nonmetallic resistivity behavior is caused by the localization effect from interstitial Fe[30,41], which is suppressed and replaced by a metallic behavior ($d\rho/dT > 0$) after removing the interstitial Fe by O_2-annealing as shown in the right panel of Fig. 4. For the annealed crystals, the AFM transition, marked by the solid magenta arrows, can be observed only in the doping region of $x \leq 0.03$, which is consistent with the results of magnetic susceptibility. For $x \geq 0.05$, the SC transition can be observed. Since the SC observed here is bulk in nature as discussed before, the positions of T_c are indicated by using solid blue arrows. It is clear that the value of T_c gradually increases with the Se doping. Here,
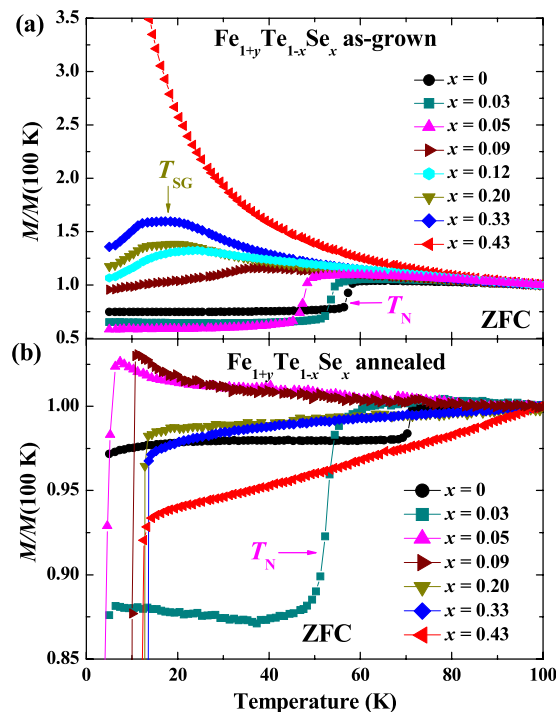
Figure 3. Magnetic susceptibilities measured at 10 kOe with $H \| c$ for $Fe_{1+y}Te_{1-x}Se_x$ ($0 \leq x \leq 0.43$) (**a**) before and (**b**) after O_2-annealing.
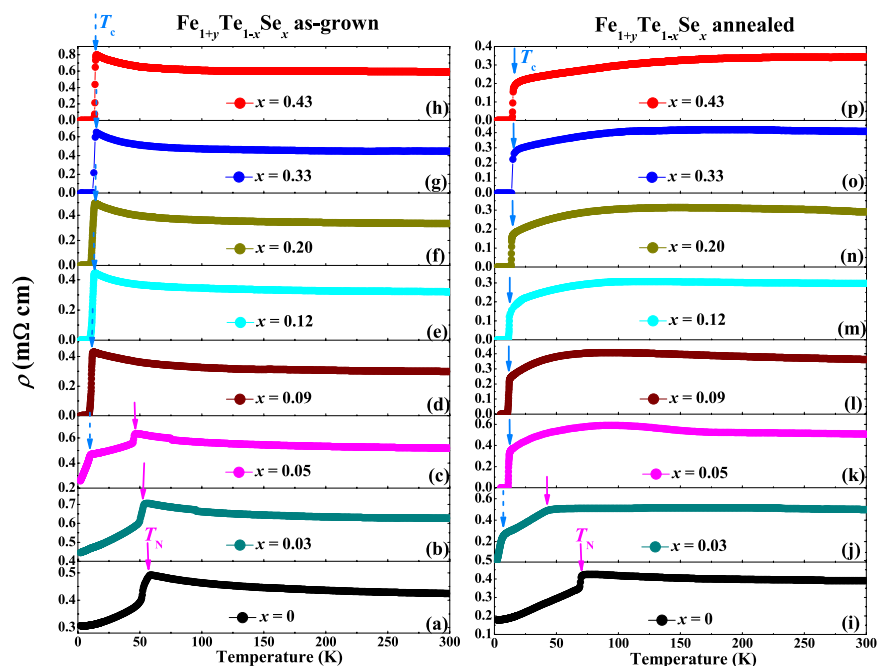
Figure 4. Temperature dependence of in-plane resistivity for the as-grown (left panel) and O_2-annealed (right panel) $Fe_{1+y}Te_{1-x}Se_x$ ($0 \leq x \leq 0.43$) single crystals. The solid magenta arrows, dashed blue arrows and solid blue arrows are used to mark the AFM, non-bulk SC, and bulk SC transitions, respectively.

we should point out that a SC-like transition at low temperature is observed in the annealed crystal with $x = 0.03$, however, the zero resistivity is not reached in the measured low temperature limit of 2 K. Such a SC transition is filamentary in nature, since it is not observed in magnetization measurements. It may come from the atomic-size fluctuation of Se doping or possible local strain effect.

To get more insight into the influence of interstitial Fe to the transport properties, temperature dependence of the Hall coefficients, R_H, for the as-grown and annealed $Fe_{1+y}Te_{1-x}Se_x$ ($0 \leq x \leq 0.43$) single crystals are measured
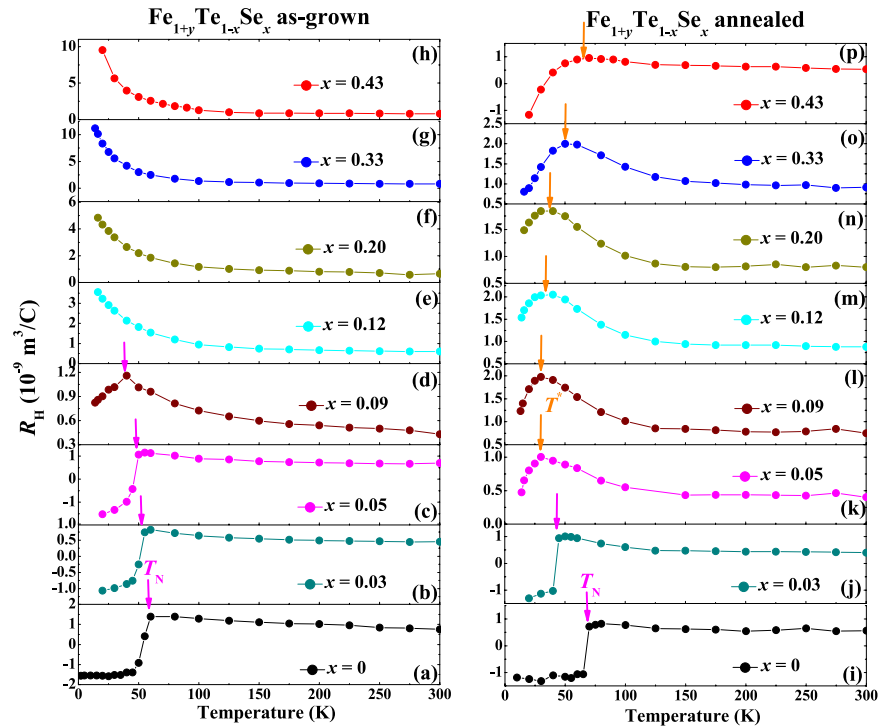
**Figure 5. Temperature dependence of Hall coefficients for the as-grown (left panel) and O$_2$-annealed (right panel) Fe$_{1+y}$Te$_{1-x}$Se$_x$ ($0 \leq x \leq 0.43$) single crystals.** The AFM transition temperatures T_N and characteristic temperature T^* were marked by the magenta and orange arrows, respectively.

and shown in Fig. 5. For the as-grown crystals, obvious AFM transition can be observed in Se doping region of $0 \leq x \leq 0.09$, and the transition temperatures T_N are indicated by the solid magenta arrows, which is consistent with the magnetic susceptibility results. For the as-grown crystal with $x = 0.09$, the AFM transition becomes much broader. Such a broader transition is also witnessed in the magnetic susceptibility measurement, which indicates that $x = 0.09$ is close to the edge of the AFM region. Since the AFM in the crystal with $x = 0.09$ is already very weak, it is not observed in the temperature dependence of resistivity measurements. The R_H for the as-grown crystals all show positive values before the AFM transition, which indicates that the hole-typed charge carriers are dominant. Besides, for $x > 0.09$, R_H shows an obvious upturn behavior with decreasing temperature below 100 K. Such upturn behavior can be also explained by the localization effect due to the presence of the interstitial Fe[30,31].

For the annealed crystals, AFM transition is only observed in the crystals with $x = 0$ and 0.03, and the value of T_N for FeTe is increased after annealing, which are all consistent with both the magnetic susceptibility and temperature dependence of resistivity measurements. For $x \geq 0.05$ (the bulk SC region), R_H keeps nearly temperature independent behavior at high temperatures, followed by a slight increase below 100 K, then suddenly decreases before reaching T_c. The value even changes the sign from positive to negative in the crystal with $x = 0.43$. The characteristic temperature at which R_H shows the maximum value before decreasing is defined as T^*, and also indicated by the solid orange arrows in the figure. It is obviously that the value of T^* gradually increases with the increase in the Se doping level. The strong temperature-dependent R_H is usually explained by the multiband nature of the sample. For the annealed Fe$_{1+y}$Te$_{1-x}$Se$_x$, hole-type charge carriers are dominant at temperatures above ~150 K, since the R_H keeps temperature independent positive value. Below ~150 K, the slight increase in R_H may come from the mobility change of the hole-type carriers or the remaining small amount of impurities formed during the removing process of the interstitial Fe (for example the FeTe$_m$[39]). Below T^*, R_H decreases with decreasing temperature, even changes the sign to negative for $x = 0.43$, which indicates that the electron-type charge carriers become more dominant. Here, we should emphasize that the T^* shows a coincident behavior with bulk T_c (T^* is observed only in the region of bulk SC, and also increased with Se doping), which indicates that the multiband nature is strongly related to the SC in Fe$_{1+y}$Te$_{1-x}$Se$_x$, and is covered up by the effect of interstitial Fe in the as-grown crystals. Actually, a very broad hump-like behavior can be observed in the ρ (T) curves for all the crystals with bulk SC, which may have similar origination as the T^* in Hall effect.

Discussion

Based on the magnetization, magnetic susceptibility, resistivity, and Hall effect measurements described above, we can establish a doping-temperature (x-T) phase diagram for the as-grown and annealed Fe$_{1+y}$Te$_{1-x}$Se$_x$ ($0 \leq x \leq 0.43$) single crystals as shown and compared in Fig. 6(a,b), respectively. For the as-grown crystals, in the doping region of $x < 0.12$, the AFM transition, ~58 K in the non-doped Fe$_{1+y}$Te, is monotonically suppressed with increasing Se substitution. More specifically in Fig. 6(a), the downtriangles, uptriangles and diamonds represent the Neel temperature T_N obtained by magnetic susceptibility, resistivity and Hall coefficient measurements. And
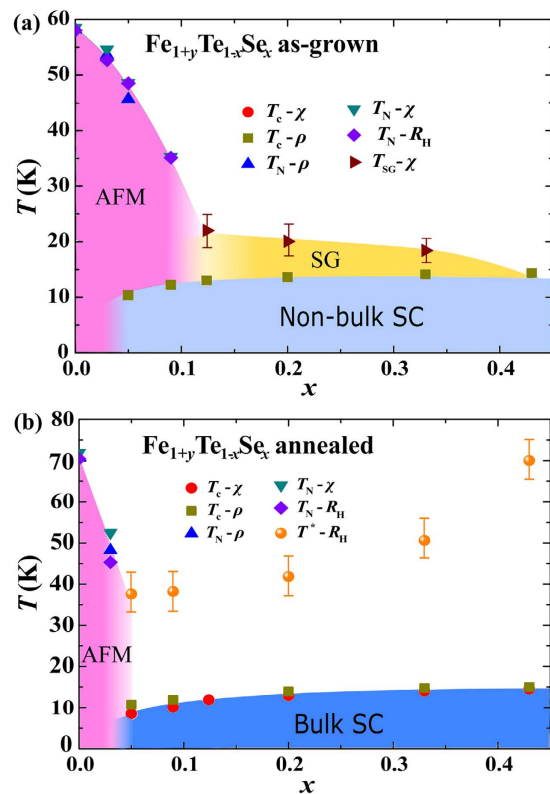
Figure 6. The doping-temperature (x-T) phase diagrams for $Fe_{1+y}Te_{1-x}Se_x$ ($0 \leq x \leq 0.43$) single crystals (**a**) before and (**b**) after O_2-annealing obtained from magnetization, magnetic susceptibility, resistivity, and Hall effect measurements.

the three disparate measurements are roughly consistent with each other. Accompanied by the suppression of AFM, SC emerges from $x = 0.05$, and coexists with the antiferromagnetic phase until $x < 0.13$. That SC, marked by the squares, is *not* bulk in nature, and can be only observed in resistivity measurement. For $x \geq 0.12$, the AFM transition is absent and replaced by a spin glass state (observed by magnetic susceptibility measurements, and marked by the righttriangles). The spin glass state is originated from the effect of interstitial Fe, which interacts with more than 50 neighboring Fe in the adjacent Fe layers, and induces the magnetic Friedel-like oscillation at $(\pi, 0)$ order[42].

After removing the interstitial Fe by O_2-annealing, the phase diagram of $Fe_{1+y}Te_{1-x}Se_x$ ($0 \leq x \leq 0.43$) is dramatically changed. As shown in Fig. 6(b), the AFM state is suppressed into a very narrow region of $x < 0.05$, and the spin glass state is totally suppressed. Immediately after the disappearance of AFM state, bulk SC emerges, and is observed in the doping region of $x \geq 0.05$. The coexistence of AFM and SC states is absent in the annealed crystals. Thus, the previously reported coexistence of AFM, spin glass state with SC may be originated from the effect of interstitial Fe. Besides, the characteristic temperature T^* observed in the R_H is plotted in the figure, which also resides in the doping region of $x \geq 0.05$, and gradually increases with increasing Se doping. It suggests that the multiband effect in $Fe_{1+y}Te_{1-x}Se_x$ may be strongly related to the occurrence of SC. On the other hand, the rapid suppression of AFM state with a small amount of doping, absence of coexistence of the AFM and SC states are all similar to the phase diagrams of $LaFeAsO_{1-x}F_x$[34] and $CeFeAsO_{1-x}F_x$[43]. This behavior is quite different from the phase diagram of "122" system[4], where the coexistence of AFM and SC is commonly observed. And the step-like behavior of the magnetism and SC in the small region of $0.03 < x < 0.05$ suggests that the SC in the $Fe_{1+y}Te_{1-x}Se_x$ system may be related to the suppression of static magnetic order rather than the increase of the effective charge carrier density by the doping or structural distortion.

In summary, the doping-temperature (x-T) phase diagrams for $Fe_{1+y}Te_{1-x}Se_x$ ($0 \leq x \leq 0.43$) single crystals before and after removing interstitial Fe by O_2-annealing are established and compared based on the systematical studies of the structure, magnetic, and transport properties. Results show that the phase diagram is largely affected by the interstitial Fe. Without interstitial Fe, the AFM state is found to be suppressed quickly with Se doping, surviving only in a narrow region of $x < 0.05$. The AFM state is proved not to coexist with the bulk SC. The previously reported spin glass state, and the coexistence of AFM and SC may be originated from the effect of interstitial Fe. Besides, a characteristic temperature T^* observed in the temperature dependent Hall coefficient in the annealed crystals is found to be accompanied by the bulk SC, which may indicate the important role of the multi-band effect in the realization of SC in this system. Future efforts on this point may be helpful to the understanding of the paring mechanism of this system.

Methods

Sample growth and annealing.   Single crystals $Fe_{1+y}Te_{1-x}Se_x$ ($0 \leq x \leq 0.43$) are grown by the self-flux method as described in detail elsewhere[41]. Single crystals with Se doping level larger than 43% cannot be grown by the flux method because of the phase separation[44]. All the crystals show plate-like morphology, with c-axis perpendicular to the plane of the plate, and can grow up to centimeter-scale. The Se/Te ratio is evaluated by the inductively-coupled plasma (ICP) atomic emission spectroscopy, and its fluctuation in different pieces obtained from the same batch is almost negligible ($\leq 1\%$). In addition, Se/Te ratio is found to change little after annealing ($\leq 1\%$). The energy dispersive x-ray spectroscopy (EDX) measurements show that Te and Se are almost homogeneously distributed in both the as-grown and annealed crystals[38]. The amount of interstitial Fe in the as-grown crystals is estimated as ~10–14% based on the ICP results. The obtained as-grown single crystals are then cut and cleaved into thin slices, and annealed with appropriate amount of O_2 at 400 °C to remove the interstitial Fe. Details about the O_2-annealing processes are reported in our previous publication[33]. Although the interstitial Fe was removed from its initial position by annealing, it may still remain in the crystal, mainly on the surface, in some form of oxides and other binary compounds. Thus, traditional compositional analysis methods like ICP, EDX and electron probe microanalyzer (EPMA) can hardly detect the change of interstitial Fe. Actually our ICP analyses on the O_2-annealed crystal show a small reduction in the Fe content after annealing. To observe the change in the amount of interstitial Fe, we employ the scanning tunneling microscopy (STM) measurements, which can directly observe the interstitial Fe in Te/Se layers. Based on our previous result on the crystal with $x = 0.43$, the values of T_c and J_c are gradually increased with removing the interstitial Fe, and reach the maximum values when the interstitial Fe are almost totally removed as observed in the STM images[33]. In the current research, all the crystals used as the annealed ones are carefully annealed by the same method to the stage with maximum T_c and J_c, which are believed to contain little interstitial Fe.

Measurements and verifications.   Details of the lattice constant change by the annealing process is characterized by means of X-ray diffraction with Cu-$K\alpha$ radiation. Magnetization measurements are performed to check the superconducting transition temperature T_c, and the susceptibility by using a commercial superconducting quantum interference device (SQUID). Longitudinal and transverse (Hall) resistivity measurements are performed by the six-lead method with a Quantum Design physical property measurement system (PPMS). In order to decrease the contact resistance, we sputter gold on the contact pads just after the cleavage. Then gold wires are attached on the contacts with silver paste. The Hall resistivity ρ_{yx} is extracted from the difference of the transverse resistance measured at positive and negative fields, i.e., $\rho_{yx}(H) = [\rho_{yx}(+H) - \rho_{yx}(-H)]/2$, which can effectively eliminate the longitudinal resistivity component due to the misalignment of contacts. Hall coefficients R_H is estimated from $R_H = \rho_{yx}/\mu_0 H$.

References

1. Kamihara, Y., Watanabe, T., Hirano, M. & Hosono, H. Iron-Based Layered Superconductor La[$O_{1-x}F_x$]FeAs ($x = 0.05$–0.12) with $T_c = 26$ K. *J. Am. Chem. Soc.* **130,** 3296 (2008).
2. Gurevich, A. Iron-based superconductors at high magnetic fields. *Rep. Prog. Phys.* **74,** 124501 (2011).
3. Scalapino, D. J. A common thread: The pairing interaction for unconventional superconductors. *Rev. Mod. Phys.* **84,** 1383 (2012).
4. Ishida, S. *et al.* Effect of Doping on the Magnetostructural Ordered Phase of Iron Arsenides: A Comparative Study of the Resistivity Anisotropy in Doped BaFe$_2$As$_2$ with Doping into Three Different Sites. *J. Am. Chem. Soc.* **135,** 3158 (2013).
5. Avci, S. *et al.* Phase diagram of Ba$_{1-x}$K$_x$Fe$_2$As$_2$. *Phys. Rev. B* **85,** 184507 (2012).
6. Kasahara, S. *et al.* Electronic nematicity above the structural and superconducting transition in BaFe$_2$(As$_{1-x}$P$_x$)$_2$. *Nature* **486,** 382 (2012).
7. Shibauchi, T., Carrington, A. & Matsuda, Y. A Quantum Critical Point Lying Beneath the Superconducting Dome in Iron Pnictides. *Annu. Rev. Cond. Mat. Phys.* **5,** 113 (2014).
8. Chen, F. *et al.* Electronic structure of Fe$_{1.04}$Te$_{0.66}$Se$_{0.34}$. *Phys. Rev. B* **81,** 014526 (2010).
9. Mazin, I. I., Singh, D. J., Johannes, M. D. & Du, M. H. Unconventional Superconductivity with a Sign Reversal in the Order Parameter of LaFeAsO$_{1-x}$F$_x$. *Phys. Rev. Lett.* **101,** 057003 (2008).
10. Kontani, H. & Onari, S. Orbital-Fluctuation-Mediated Superconductivity in Iron Pnictides: Analysis of the Five-Orbital Hubbard-Holstein Model. *Phys. Rev. Lett.* **104,** 157001 (2010).
11. Hsu, F.-C. *et al.* Superconductivity in the PbO-type structure α-FeSe. *Proc. Nat. Acad. Sci.* **105,** 14262 (2008).
12. Sales, B. C. *et al.* Bulk superconductivity at 14 K in single crystals of Fe$_{1+y}$Te$_x$Se$_{1-x}$. *Phys. Rev. B* **79,** 094521 (2009).
13. Margadonna, S. *et al.* Pressure evolution of the low-temperature crystal structure and bonding of the superconductor FeSe ($T_c = 37$K). *Phys. Rev. B* **80,** 064506 (2009).
14. Medvedev, S. *et al.* Electronic and magnetic phase diagram of β-Fe$_{1.01}$Se with superconductivity at 36.7 K under pressure. *Nat. Mater.* **8,** 630 (2009).
15. Guo, J. *et al.* Superconductivity in the iron selenide K$_x$Fe$_2$Se$_2$ ($0 \leq x \leq 1.0$). *Phys. Rev. B* **82,** 180520 (2010).
16. Burrard-Lucas, M. *et al.* Enhancement of the superconducting transition temperature of FeSe by intercalation of a molecular spacer layer. *Nat. Mater.* **12,** 15 (2013).
17. Sun, L. *et al.* Re-emerging superconductivity at 48 kelvin in iron chalcogenides. *Nature* **483,** 67–69 (2012).
18. Ge, J.-F. *et al.* Superconductivity above 100 K in single-layer FeSe films on doped SrTiO$_3$. *Nat Mater* **14,** 285–289 (2015).
19. Bao, W. *et al.* Tunable (δπ, δπ)-Type Antiferromagnetic Order in α-Fe(Te, Se) Superconductors. *Phys. Rev. Lett.* **102,** 247001 (2009).
20. Paglione, J. & Greene, R. L. High-temperature superconductivity in iron-based materials. *Nat Phys* **6,** 645 (2010).
21. Katayama, N. *et al.* Investigation of the Spin-Glass Regime between the Antiferromagnetic and Superconducting Phases in Fe$_{1+y}$Se$_x$Te$_{1-x}$. *J. Phys. Soc. Jpn.* **79,** 113702 (2010).
22. Noji, T. *et al.* Growth, Annealing Effects on Superconducting and Magnetic Properties, and Anisotropy of FeSe$_{1-x}$Te$_x$ ($0.5 \leq x \leq 1$) Single Crystals. *J. Phys. Soc. Jpn.* **79,** 084711 (2010).
23. Liu, T. J. *et al.* From (π, 0) magnetic order to superconductivity with (π, π) magnetic resonance in Fe$_{1.02}$Te$_{1-x}$Se$_x$. *Nat. Mater.* **9,** 718 (2010).
24. Dong, C. *et al.* Revised phase diagram for the FeTe$_{1-x}$Se$_x$ system with fewer excess Fe atoms. *Phys. Rev. B* **84,** 224506 (2011).
25. Kawasaki, Y. *et al.* Phase diagram and oxygen annealing effect of FeTe$_{1-x}$Se$_x$ iron-based superconductor. *Solid State Commun.* **152,** 1135 (2012).
26. Zhuang, J. C. *et al.* Enhancement of transition temperature in Fe$_x$Se$_{0.5}$Te$_{0.5}$ film via iron vacancies. *Appl. Phys. Lett.* **104,** 262601 (2014).

27. Imai, Y., Sawada, Y., Nabeshima, F. & Maeda, A. Suppression of phase separation and giant enhancement of superconducting transition temperature in $FeSe_{1-x}Te_x$ thin films. *Proc. Nat. Acad. Sci.* **112,** 1937 (2015).
28. Bendele, M. *et al.* Tuning the superconducting and magnetic properties of $Fe_ySe_{0.25}Te_{0.75}$ by varying the iron content. *Phys. Rev. B* **82,** 212504 (2010).
29. Zhang, L., Singh, D. J. & Du, M. H. Density functional study of excess Fe in $Fe_{1+x}Te$: Magnetism and doping. *Phys. Rev. B* **79,** 012506 (2009).
30. Liu, T. J. *et al.* Charge-carrier localization induced by excess Fe in the superconductor $Fe_{1+y}Te_{1-x}Se_x$. *Phys. Rev. B* **80,** 174509 (2009).
31. Sun, Y. *et al.* Multiband effects and possible Dirac fermions in $Fe_{1+y}Te_{0.6}Se_{0.4}$. *Phys. Rev. B* **89,** 144512 (2014).
32. Wen, J., Xu, G., Gu, G., Tranquada, J. M. & Birgeneau, R. J. Interplay between magnetism and superconductivity in iron-chalcogenide superconductors: crystal growth and characterizations. *Rep. Prog. Phys.* **74,** 124503 (2011).
33. Sun, Y. *et al.* Dynamics and mechanism of oxygen annealing in $Fe_{1+y}Te_{0.6}Se_{0.4}$ single crystal. *Sci. Rep.* **4,** 4585 (2014).
34. Luetkens, H. *et al.* The electronic phase diagram of the $LaO_{1-x}F_xFeAs$ superconductor. *Nat. Mater.* **8,** 305–309 (2009).
35. Fang, M. H. *et al.* Superconductivity close to magnetic instability in $Fe(Se_{1-x}Te_x)_{0.82}$. *Phys. Rev. B* **78,** 224503 (2008).
36. Rodriguez, E. E. *et al.* Chemical control of interstitial iron leading to superconductivity in $Fe_{1+x}Te_{0.7}Se_{0.3}$. *Chem. Sci.* **2,** 1782 (2011).
37. Sun, Y. *et al.* Large, Homogeneous, and Isotropic Critical Current Density in Oxygen-Annealed $Fe_{1+y}Te_{0.6}Se_{0.4}$ Single Crystal. *Appl. Phys. Express* **6,** 043101 (2013).
38. Sun, Y. *et al.* Evolution of superconducting and transport properties in annealed $FeTe_{1-x}Se_x$ $(0.1 \leq x \leq 0.4)$ multiband superconductors. *Supercond. Sci. Technol.* **28,** 044002 (2015).
39. Lin, W. *et al.* Role of chalcogen vapor annealing in inducing bulk superconductivity in $Fe_{1+y}Te_{1-x}Se_x$. *Phys. Rev. B* **91,** 060513 (2015).
40. Yamada, T., Sun, Y., Pyon, S. & Tamegai, T. Effects of Pnictogen Atmosphere Annealing on $Fe_{1+y}Te_{0.6}Se_{0.4}$. *J. Phys. Soc. Jpn.* **85,** 024712 (2016).
41. Sun, Y., Taen, T., Tsuchiya, Y., Shi, Z. X. & Tamegai, T. Effects of annealing, acid and alcoholic beverages on $Fe_{1+y}Te_{0.6}Se_{0.4}$. *Supercond. Sci. Technol.* **26,** 015015 (2013).
42. Thampy, V. *et al.* Friedel-Like Oscillations from Interstitial Iron in Superconducting $Fe_{1+y}Te_{0.62}Se_{0.38}$. *Phys. Rev. Lett.* **108,** 107002 (2012).
43. Zhao, J. *et al.* Structural and magnetic phase diagram of $CeFeAsO_{1-x}F_x$ and its relation to high-temperature superconductivity. *Nat. Mater.* **7,** 953 (2008).
44. Mizuguchi, Y. & Takano, Y. Review of Fe Chalcogenides as the Simplest Fe-Based Superconductor. *J. Phys. Soc. Jpn.* **79,** 102001 (2010).

Acknowledgements

Author Contributions

Y.S. performed most of the experiments and analyzed the data. T.Y. and S.P. contributed to the XRD measurement. Y.S. and T.T. designed the research. Most of the text of the paper was written jointly by Y.S. and T.T. All the authors contributed to discussion on the results for the manuscript.

Additional Information